บรรณานุกรม

1. Wolf, S. A., Awschalom, D. D., Buhnrman, R. A., Daughton, J. M., Von Molnar, S., Roukes, M. L., Chtchelkanova, A. Y. and Treger D. M. 2001. Spintronics: A Spin based electronics vision for the future. Science. 16 : 1488-1495.
2. Pearton, S. J., Abernathy, C. R., Norton, D. P., Hebard, A. F., Park, Y. D., Boatner, L. A. and Budai, J. D. 2003. Advances in wide band gap materials for semiconductor Spintronics. Materials Science and Engineering. 40 : 137-168.
3. Greenwood, N. N. and Earnshaw, A. 1997. Chemistry of the Elements, 3rd edition, Butterworth, UK.
4. Shannon, R. D. and Prewitt, C. T. 1979. Effective ionic radii in oxides and fluorides. Acta Crystallographica. A32 : 751-767.
5. Sarma, S. D. 2001. Spintronics A new class of device based on the quantum of electron spin, rather than on charge, may yield the next generation of microelectronics. American Scientist. 89 : 516-523.
6. Ohno, H. 1998. Making Nonmagnetic Semiconductors Ferromagnetic. Science. 281 : 951-956.
7. Dietl, T., Ohno, H., Matsukura, F., Cibert, J.and Ferrand, D. 2000. Science. 287 : 1019-1022.
8. Fukumura T., Zhengwu J. T., Ohtomo, A., Koinuma, H. and Kawasaki, M. 1999. An oxide-diluted magnetic semiconductor : Mn-doped ZnO. Applied Physics Letters. 75 : 3366-3368.
9. Kim, J.-H., Kim, H., Kim, D., Ihm, Y.-E. and Choo, W.-K. 2002. Magnetic properties of epitaxially grown semiconducting $Zn_{1-x}Co_xO$ thin films by pulsed laser deposition. Journal of Applied Physics. 92 : 6066-6071.
10. Tiwari, A., Jin, C., Kvit, A., Kumar, D., Muth, J. F. and Narayan, J. 2002. Structural, optical and magnetic properties of diluted magnetic semiconducting $Zn_{1-x}Mn_xO$ film. Solid State Communications. 121 : 371-374 .
11. Wakano, T., Fujimura, N., Morinaga, Y., Abe, N., Ashida, A., and Ito, T. 2001. Magnetic and magneto-transport properties of ZnO: Ni films. Physica E. 10 : 260-264.
12. Saeki, H., Tabata, H. and Kawai, T. 2001. Magnetic and electric properties of vanadium doped ZnO films. Solid State Communications. 120 :439-443.

13. Jung, S. W., An, S.-J., Yi, G.-C., Jung, C. U., Lee, S.-I. and Cho, S. 2002. Ferromagnetic properties of $Zn_{1-x}Mn_xO$ epitaxial thin films. Applied Physics Letters. 80 : 4561-4563.

14. Han, S.-J., Song, J. W., Yang, C.-H., Park, S. H., Park, J.-H., Jeong, Y. H. and Rhie, K. W. 2002. A key to room-temperature ferromagnetism in Fe-doped ZnO: Cu. Applied Physics Letters. 81 : 4212-4214.

15. Sharma, P., Gupta, A., Rao, K. V., Owens, F. J., Sharma, R., Ahuja, R., Guillen, J. M. O., Johansson, B. and Gehring, G. A. 2003. Ferromagnetism above room temperature in bulk and transparent thin films of Mn-doped ZnO. Nature materials. 2 : 673-677.

16. Matsumoto, Y., Murakami, Y. M., Shono, T., Hasegawa, T., Fukumura, T., Kawasaki, M., Ahmet, P., Chikyow, T., Koshihara, S.-y. and Koinuma, H. 2001. Room-Temperature Ferromagnetism in Transparent Transition Metal-Doped Titanium Dioxide. Science. 291 : 854-856.

17. Shinde, S. R., Ogale, S. B., Das Sarma, S., Simpson, J. R., Drew, H. D., Lofland, S. E., Lanci, C. Buban, J. P., Browning, N. D., Kulkarni, V. N., Higgins, J. Sharma, R. P., Greene, R. L. and Venkatesan, T. 2003. Ferromagnetism in laser deposited anatase $Ti_{1-x}Co_xO_{2-\delta}$ films . Physical Review B. 67, 1152111-1152116.

18. Stampe, P. A., Kennedy, R. J., Xin, Y. and Parker, J. S. 2003. Investigation of the cobalt distribution in the room temperature ferromagnet TiO_2:Co. Journal of Applied. Physics. 93(10) : 7864-7866.

19. Matsumoto, Y., Takahashi, R., Murakami, M., Koida, T., Fan, X.-J., Hasegawa, T., Fukumura, T., Kawasaki, M., Koshihara, S. and Koinuma, H. 2001. Japanees Journal of Applied. Physics. 40 : L1204.

20. Kimura, H., Fukumura, T., Kawasaki, M., Inaba, K., Hasekawa, T. and Koinuma, H. 2002. Rutile-type oxide-diluted magnetic semiconductor: Mn-doped SnO_2. Applied Physics Letters. 80(1) : 94-96.

21. Ogale, S. B., Choudhary, R. J., Buban, J. P., Lofland, S. E., Shinde, S. R., Kale, S. N., Kulkarni, V. N., Higgins, J., Lanci, C., Simpson, J. R., Browning, N. D., Das Sarma, S., Drew, H. D., Greene, R. L. and Venkatesan, T. 2003. High Temperature Ferromagnetism with a Giant Magnetic Moment in Transparent Co-doped SnO_2. Physical Review Letters. 91 : 077205/1-4.

22. Coey, J. M. D., Douvalis, A.P., Fitzgerald, C. B. and Venkatesan, M. 2004. Ferromagnetism in Fe-doped SnO_2 thin films. Applied Physics Letters. 85 : 1332-1334.

23. Kim, E. C., Moon, S. H., Woo, S. I., Cho, J. H., Joh, Y. G. and Kim, D. H. 2004. Mössbauer study and magnetic properties of $Ti_{0.99}{}^{57}Fe_{0.01}O_2$. Solid state communications. 132 : 477-480.

24. Punnoose, A., Hays, J., Gopal, V. and Shutthanandan, V. 2004. Room-temperature ferromagnetism in chemically synthesized $Sn_{1-x}Co_xO_2$ powders. Applied Physics Letters. 85 : 1559-1561.

25. Punnoose, A. and Hays, J. 2005. Possible metamagnetic oigin of ferromagnetism in transition-metal-doped SnO_2. Journal of Applied Physics. 97 : 10D321-1-3.

26. Fitzgerald, C. B., Venkatesan, M., Douvalis, A. P., Huber, S., Coey, J. M. D. and Bakas, T. 2004. SnO_2 doped with Mn, Fe or Co: Room temperature dilute magnetic semiconductors. Journal of Applied Physics. 95 : 7390-7392.

27. Hong, N. H., Sakai, J., Prellier, W. and Hassini, A. 2005. Transparent Cr-doped SnO_2 thin films: ferromagnetism beyond room temperature with a giant magnetic moment. Journal of Physics : condensed matter. 17 : 1697-1702.

28. Hong, N. H.and Sakai, J. 2005. Ferromagnetic V-doped SnO_2 thin films. Physica B. 358 : 265–268.

29. Hong, N. H., Ruyter, A., Prellier, W., Sakai, Joe. and Huong, N. T. 2005. Magnetism in Ni-doped SnO_2 thin films. Journal of Physics : condensed matter. 17 : 6533-6538.

30. Punnoose, A., Hays, J., Thurber, A., Engelhard, M. H., Kukkadapu, R. K., Wang, C., Shutthanandan, V. and Thevuthasan, S. 2005. Development of high-temperature ferromagnetism in SnO_2 and paramagnetism in SnO by Fe doping. Physical Review B. 72 : 054402/1-14.

31. Archer, P. I., Radovanovic, P. V., Heald, S. M. and Gamelin, D. R. 2005. Low-Temperature Activation and Deactivation of High-Curie-Temperature Ferromagnetism in a New Diluted Magnetic Semiconductor: Ni^{2+}-Doped SnO_2. Journal American Chemical Society. 127: 14479-14487.

32. .Young R. A. 1993 The Rietveld Method. International Union of Crystallography, Oxford University Press.

33. Rodríguez-Carvajal J. 1993 "Recent advances in Magnetic Structure Determination by Neutron Powder Diffraction", Physica B: Condensed Matter. 192, 55–69.

34. Scherrer, P. 1918. Bestimmung der Grosse und der Inneren Struktur von Kolloid. teilchen mittels Rontgenstrahlen. Nachrichten aus der Göttingen. 2 : 98-100.

35. Williamson, G. K. and Hall, W. H. 1953. X-Ray Line Broadening from Filed Aluminium and Wolfram. Acta Metallurgica. 1 : 22-31.

36. Wertheim, G. K., Butler, M. A., West, K. W. and Buchanan, D. N. E. 1974. Determination of the Gaussian and Lorentzian content of experimental line shapes. Review of Scientific Instrumental. 45 : 1369-1371.

37. Cheary, R. W. and Coelho, A. A. 1996 .Programs XFIT and FOURYA, deposited in CCP14 Powder Diffraction Library, Engineering and Physical Sciences Research Council, Daresbury Laboratory, Warrington, England.

38. .Suryanarayana C. and Grant Norton M. 1998 X-ray Diffraction: A Practical Approach. New York: Plenum Press.

39. .Ren F. and et al. 1992 Chromium-based Ceramic Colors, Ceramic Bullatin. 71, 759–764.

40. Kittel C. 1996 Introduction to Solid State Physics. 7^{th} edition. New York: Wiley.

41. Bouaine A. and et al. 2007 Structural, Optical, and Magnetic Properties of Co–doped SnO_2 Powders Synthesized by the Coprecipitation Technique. Journal of Physical Chemistry C. 111, 2924–2928.

42. Bucher J. P., Douglass D. C., and Bloomfield L. A. 1991 Magnetic Properties of Free Cobalt Clusters. Physical Review Letters. 66, 3052–3055.

43. Fang L. M. and et al. 2008 Synthesis and Characteristics of Fe^{3+}–doped SnO_2 nanoparticles via sol–gel–calcination or sol–gel–hydrothermal route. Journal of Alloys and Compounds. 454, 261–267.

ภาคผนวก

ตัวอย่างการคำนวณขนาดผลึกของ $Sn_{0.700}Fe_{0.300}O_{2-\delta}$ เผาแคลไซน์ที่ 700 °C

ตาราง ผ.1 ค่า β_i ของ commercial SnO_2 เผาแคลไซน์ที่ 1000 °C 3 ชั่วโมง

Material: Commercial SnO_2			Radiation: CuKα, λ= 0.15418 nm
2theta (degree)	*hkl*	FWHM (degree)	FWHM (rad) = β_i
26.5866	110	0.2214	3.86×10^{-3}
33.8632	101	0.2155	3.76×10^{-3}
37.9406	200	0.1938	3.38×10^{-3}
51.8138	211	0.1876	3.27×10^{-3}
54.8148	220	0.1776	3.10×10^{-3}

ตาราง ผ.2 ขนาดผลึกของ $Sn_{0.700}Fe_{0.300}O_{2-\delta}$ คำนวณโดยสมการ Scherrer

Material: $Sn_{0.70}Fe_{0.30}O_{2-\delta}$				Radiation: CuKα, λ= 0.15418 nm		
2θ (°)	*hkl*	β_o (°)	β_o (rad)	$\beta_r = \sqrt{(\beta_o - \beta_i)\sqrt{(\beta_o^2 - \beta_i^2)}}$	$\beta_r \cos\theta$	<*D*> (nm)
26.61	110	1.32	2.31×10^{-2}	2.10×10^{-2}	2.04×10^{-2}	6.82
33.94	101	1.17	2.04×10^{-2}	1.82×10^{-2}	1.75×10^{-2}	7.95
38.04	200	1.33	2.32×10^{-2}	2.13×10^{-2}	2.01×10^{-2}	6.89
51.91	211	1.40	2.44×10^{-2}	2.26×10^{-2}	2.03×10^{-2}	6.82
54.85	220	1.39	2.42×10^{-2}	2.25×10^{-2}	2.00×10^{-2}	6.95
						7.09± 0.44

ตาราง ผ.3 ขนาดผลึกของ $Sn_{0.700}Fe_{0.300}O_{2-\delta}$ คำนวณโดยเทคนิค Williamson-Hall Plot method

Material: $Sn_{0.70}Fe_{0.30}O_{2-\delta}$				Radiation: CuKα, λ= 0.15418 nm		
2θ (°)	*hkl*	β_o (°)	β_o (rad)	$\beta_r = \sqrt{(\beta_o - \beta_i)\sqrt{(\beta_o^2 - \beta_i^2)}}$	$\beta_r \cos\theta$	$4\sin\theta$
26.61	110	1.32	2.31×10^{-2}	2.10×10^{-2}	2.04×10^{-2}	0.92
33.94	101	1.17	2.04×10^{-2}	1.82×10^{-2}	1.75×10^{-2}	1.17
38.04	200	1.33	2.32×10^{-2}	2.13×10^{-2}	2.01×10^{-2}	1.30
51.91	211	1.40	2.44×10^{-2}	2.26×10^{-2}	2.03×10^{-2}	1.75
54.85	220	1.39	2.42×10^{-2}	2.25×10^{-2}	2.00×10^{-2}	1.84

Plot $\beta_r \cos\theta$ versus $4\sin\theta$

ขนาดผลึกคำนวณโดยสมการ Scherrer และเทคนิค Williamson–Hall Plot

ตาราง ผ.4 ขนาดผลึก *D* (nm) ของ $Sn_{1-x}Cr_xO_{2-\delta}$

x	Scherrer's equation			WHP method		
	500 °C	600 °C	700 °C	500 °C	600 °C	700 °C
0.000	10.31 ± 0.56	12.39 ± 0.63	14.48 ± 0.69	12.58 ± 0.46	16.04 ± 0.18	18.27 ± 0.29
0.005	6.96 ± 0.73	12.19 ± 0.45	15.76 ± 0.20	5.71 ± 0.99	12.20 ± 0.71	20.05 ± 0.43
0.010	6.67 ± 0.77	10.55 ± 0.58	13.22 ± 0.82	6.31 ± 0.86	13.22 ± 0.43	19.97 ± 0.24
0.015	6.73 ± 0.67	10.32 ± 0.59	12.98 ± 0.67	8.21 ± 0.34	13.22 ± 0.26	19.20 ± 0.18

ตาราง ผ.5 ขนาดผลึก *D* (nm) ของ $Sn_{1-x}Co_xO_{2-\delta}$

x	Scherrer's equation			WHP method		
	500 °C	600 °C	700 °C	500 °C	600 °C	700 °C
0.005	5.99 ± 0.33	10.27 ± 0.37	12.62 ± 0.55	5.17 ± 0.35	10.46 ± 0.56	16.09 ± 0.90
0.010	5.72 ± 0.41	9.03 ± 0.34	11.69 ± 0.37	5.56 ± 0.29	11.08 ± 0.43	15.32 ± 0.84
0.015	5.68 ± 0.36	8.73 ± 0.42	11.22 ± 0.43	5.82 ± 0.59	10.18 ± 0.61	14.43 ± 0.85

ตาราง ผ.6 ขนาดผลึก *D* (nm) ของ $Sn_{1-x}Fe_xO_{2-\delta}$

x	Scherrer's equation			WHP method		
	500 °C	600 °C	700 °C	500 °C	600 °C	700 °C
0.005	5.83 ± 0.60	11.18 ± 0.47	15.05 ± 0.96	6.71 ± 0.86	14.40 ± 0.08	20.70 ± 0.17
0.010	5.86 ± 0.57	11.55 ± 0.40	15.47 ± 0.83	6.57 ± 0.94	14.32 ± 0.14	20.89 ± 0.10
0.015	5.39 ± 0.52	10.11 ± 0.48	14.96 ± 0.42	5.51 ± 0.74	12.30 ± 0.39	18.05 ± 0.20
0.100	5.22 ± 0.32	8.00 ± 0.42	10.95 ± 0.55	5.88 ± 0.91	9.41 ± 0.64	13.41 ± 0.41
0.150	5.14 ± 0.30	7.47 ± 0.39	9.78 ± 0.55	5.81 ± 0.88	8.53 ± 0.81	11.76 ± 0.55
0.200	4.84 ± 0.34	6.19 ± 0.47	7.94 ± 0.33	5.27 ± 0.93	7.67 ± 0.28	9.06 ± 0.79
0.250	4.85 ± 0.38	5.84 ± 0.44	7.30 ± 0.36	5.29 ± 0.95	6.98 ± 0.66	8.49 ± 0.67
0.300	4.41 ± 0.39	5.38 ± 0.39	7.09 ± 0.44	4.59 ± 0.77	6.13 ± 0.86	8.34 ± 0.67

ผลลัพธ์งานวิจัย

ผลลัพทธ์	ทางตรง (หน่วยนับ)
องค์ความรู้	-การเตรียมอนุภาคนาโนโลหะทรานซิชันเจือสารกึ่งตัวนำทินออกไซด์โดยเทคนิคออโตคอมบัสชัน -สมบัติทางกายภาพ สมบัติเชิงแสง และสมบัติแม่เหล็กของอนุภาคนาโนโลหะทรานซิชันเจือสารกึ่งตัวนำทินออกไซด์
บทความทางวิชาการ	Wenger LE, Tsoi GM, Suryanarayanan R, and Sudyoadsuk T 2008 Effect of Cr-doping on the magnetic and electrical properties of $La_{0.4}Ca_{0.6}MnO_3$ Journal of Applied Physics.**103**, 7, 07F723
เอกสารประกอบการประชุม/สัมมนาในและต่างประเทศ	Taweesak Sudyoadsuk, Malee Prajuabsuk and Pongtip Winotai Tuning the Band gap energy of SnO_2 by Substitution with Fe^{3+} Proceeding at 33rd Congress on Science and Technology of Thailand Walailak University, Thailand, 18 - 20 October 2007
การผลิตบุคคลากร นักศึกษาปริญญาตรี นักศึกษาปริญญาโท	 นายวิทวัฒน์ ขันติวงศ์ นายศักดิ์ชัย วงศ์เพ็ง นางสาวกมลวรรณ รินทรามี และนางสาวสุรัตดา ศรีสุวรณ์ นางสาวมาลี ประจวบสุข
เอกสารทางวิชาการรายงานฉบับสมบูรณ์	เรื่อง สมบัติเฟอร์โรแมกเนติก ณ อุณหภูมิห้อง ของสารประกอบเซมิคอนดักเตอร์ทินออกไซด์ที่มีโลหะทรานซิชันเป็นตัวเติม สำหรับเทคโนโลยีสปินทรอนิกส์
สารนิพนธ์ นักศึกษาปริญญาตรี	เรื่องการเตรียมอนุภาคขนาดนาโนเมตรของโครเมียมเจือทินออกไซด์โดยเทคนิคออโตคอมบัสชัน โดย นายวิทวัฒน์ ขันติวงศ์ และนายศักดิ์ชัย วงศ์เพ็ง เรื่องการเตรียมผลึกขนาดนาโนเมตรของเหล็กเจือทิน(IV) ออกไซด์โดยเทคนิคออโตคอมบัสชัน โดย นางสาวกมลวรรณ รินทรามี และนางสาวสุรัตดา ศรีสุวรณ์
วิทยานินธ์ นักศึกษาปริญญาโท	เรื่อง การศึกษาสมบัติของสารประกอบอนุภาคนาโนทินออกไซด์ ที่มีโลหะทรานสิชันเป็น ตัวเติม เตรียมโดยเทคนิคออโตคอมบัสชัน โดย นางสาวมาลี ประจวบสุข

ภาคผนวก

1. Wenger LE, Tsoi GM, Suryanarayanan R, and Sudyoadsuk T 2008 Effect of Cr-doping on the magnetic and electrical properties of $La_{0.4}Ca_{0.6}MnO_3$ Journal of Applied Physics.**103**, 7, 07F723

2. Taweesak Sudyoadsuk, Malee Prajuabsuk and Pongtip Winotai Tuning the Band gap energy of SnO_2 by Substitution with Fe^{3+} Proceeding at 33rd Congress on Science and Technology of Thailand Walailak University, Thailand, 18 - 20 October 2007

Effect of Cr-doping on the magnetic and electrical properties of $La_{0.4}Ca_{0.6}MnO_3$

L. E. Wenger,[1,a] G. M. Tsoi,[1] R. Suryanarayanan,[2] and T. Sudyoadsuk[3]
[1]*Department of Physics, The University of Alabama at Birmingham, Birmingham, Alabama 35294, USA*
[2]*Laboratoire de Physico-Chimie de l'Etat Solide, CNRS, Université Paris-Sud, 91405 Orsay, France*
[3]*Department of Chemistry, Ubon Ratchathani University, Ubon Ratchathani 34190, Thailand*

(Presented on 8 November 2007; received 12 September 2007; accepted 4 December 2007; published online 18 March 2008)

The magnetic and electrical properties of electron-doped manganite $La_{0.4}Ca_{0.6}Mn_{1-y}Cr_yO_3$ polycrystalline samples ($y=0.02$, 0.04, and 0.06) prepared by a sol-gel technique have been investigated between 5 and 325 K in magnetic fields ranging from 0 to 5 T. Both the *M-T* and *M-H* data indicate that these Cr-doped manganites exhibit multiple ferromagnetic phases in which the relative amounts of each phase and temperatures of their appearance change with Cr content. The temperature dependence of the zero-field resistivity indicates that a transition occurs below 150 K from an insulating (semiconducting) behavior to a behavior exhibiting a temperature-independent plateau with the magnitude of a semimetal. In addition a large field-induced behavior is found in both the magnetoresistance and magnetization at temperatures correlated to the ferromagnetic semimetallic phase being induced, which results in a large magnetoresistance at the lowest temperatures. © *2008 American Institute of Physics.*
[DOI: 10.1063/1.2838625]

I. INTRODUCTION

Recently, substituting the manganese sites in mixed manganites of $La_{1-x}Ca_xMnO_3$ with various other 3-*d* metallic cations[1,2] has been shown to suppress the charge ordering (CO) in various electron-doped manganites and to exhibit interesting properties including insulator-to-metal (I/M) transitions and large magnetoresistance effects. Cr substitution[3–5] is particularly interesting as Cr^{3+} is isoelectronic with Mn^{4+} and is a non–Jahn–Teller ion. In addition, the magnetic interaction Cr^{3+}–O–Mn^{3+} is known to favor ferromagnetism through the superexchange mechanism. To date, most studies have focused on the effect of Cr-doping on the properties of the $x=0.5$ manganites (commensurate CO insulators) which typically result in the appearance of a ferromagnetic metal (FMM) state at low temperatures in zero magnetic field with the gradual suppression of the CO state with increasing Cr content. Similar behavior[6] was observed on a Ca-rich manganite system, $Pr_{1-x}Ca_xMnO_3$ ($0.6 \leq x \leq 0.7$), in which the complete suppression of the CO state occurred above 10% Cr along with the appearance of a reentrant *I/M* transition in the 90–120 K temperature range. Also colossal magnetoresistance (CMR) effects were induced by the application of strong magnetic fields for samples with 7% Cr or greater. Hence, similar studies investigating the effect of Cr substitutions on the structural, magnetic, and electrical transport properties of the Ca-rich $La_{1-x}Ca_xMnO_3$ system can be enlightening for comparison. With this in mind, this paper reports on dc magnetization and magnetoresistance measurements on polycrystalline samples of $La_{0.40}Ca_{0.60}Mn_{1-y}Cr_yO_3$ ($0.02 \leq y \leq 0.06$).

[a]Electronic mail: wenger@uab.edu.

II. EXPERIMENT

Polycrystalline samples of nominal $La_{0.40}Ca_{0.60}Mn_{1-y}Cr_yO_3$ composition with $y=0.02$, 0.04, and 0.06 were prepared by a sol-gel technique. Stoichiometric amounts of $La(NO_3)_3 \cdot 6H_2O$ (99%), $CaCO_3$ (99.5%), $Cr(NO_3)_3 \cdot 9H_2O$ (97%), and $Mn(CH_3COO)_2 \cdot 4H_2O$ (99%) were dissolved in a dilute HNO_3 solution with citric acid and ethylene glycol used as the chelating agents. The mixed solution was then heated until a dark-brown-colored resin material was formed. The resin was subsequently fired at 727 and 1127 K in air to decompose the organic residue. The resultant powder was then ground, pelletized, and sintered at 1527 K for 12 h.

Room-temperature powder x-ray diffraction patterns for these samples were indexed to the $GdFeO_3$-perovskite structure with the space group *Pbnm* and did not show the presence of any impurity phases or precipitates of unreacted oxides. The cell volume of these samples decreased with increasing Cr substitution which can be attributed to the smaller ionic radius of the Cr^{3+} ion than that of the Mn^{3+} ion. The dc magnetization (M) measurements as a function of temperature ($5 \leq T \leq 325$ K) and magnetic field ($0 \leq H \leq 5$ T) were performed using a commercial Quantum Design superconducting quantum interference device magnetometer model MPMS-5S. The dc electrical resistivity ρ as a function of T and H was measured by a standard four-probe method with silver paint used to make electrical contacts to the ceramic samples.

III. RESULTS AND DISCUSSION

The temperature dependences of the magnetization M/H for the smallest Cr-doped ($y=0.02$) sample are presented in

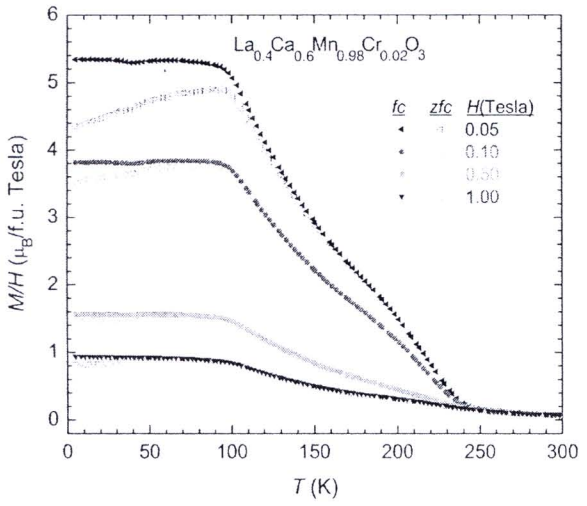

FIG. 1. (Color online) The dc magnetic susceptibility M/H of $La_{0.40}Ca_{0.60}Mn_{0.98}Cr_{0.02}O_3$ as a function of temperature T. Both the field-cooled (fc) and zero-field-cooled (zfc) data are shown for different magnetic field strengths H.

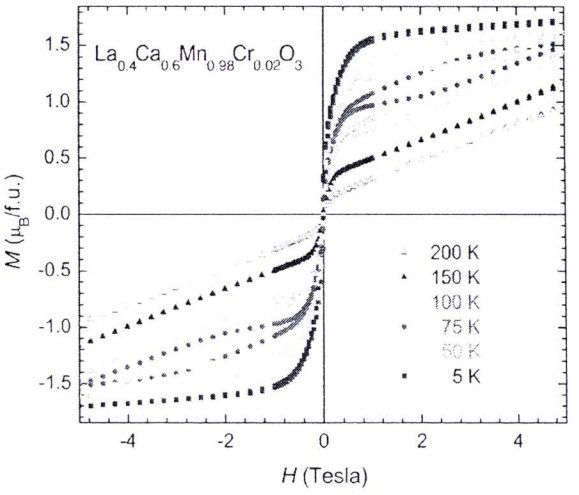

FIG. 2. (Color online) Field dependence of the magnetization M of $La_{0.40}Ca_{0.60}Mn_{0.98}Cr_{0.02}O_3$ at various temperatures.

Fig. 1 for various magnetic fields. From the 0.05 T data, three fairly distinct features can be identified as being the onset of different magnetic regimes or phases: (i) the magnetization increases rather rapidly at 240 K followed by (ii) the appearance of a second increase in the magnetization below 150 K. The magnetization eventually flattens out into a nearly temperature-independent magnetization below 100 K, and (iii) then a barely perceptive "bump" appears in the field-cooled magnetization around 40 K. Irreversibility between the field-cooled and zero-field-cooled data is observable below 150 K which progressively diminishes and whose onset occurs at lower temperatures with increasing magnetic field strengths until it is only visible below 40 K at the highest applied field. While the magnetic response at 240 K has the characteristic temperature behavior associated with ferromagnetic ordering, it is uncertain whether the second magnetization increase occurring below 150 K results from a ferromagnetic ordering of a separate microscopic magnetic phase or from the 240 K phase experiencing a different type of ferromagnetic ordered structure. The nature of these two magnetic phases will become even more evident after examining the M-H and ρ-T results described in the subsequent paragraph. The magnetic state or phase associated with the 40 K is less certain, but it is reasonable to surmise that it is also associated with another ferromagnetic ordered region or ferromagnetic frozen cluster state. Lastly the paramagnetic-to-CO transition observed at 260 K in the parent $La_{0.40}Ca_{0.60}MnO_3$ compound is completely suppressed with just a 2% Cr substitution, or at least the characteristic sharp magnetization peak accompanying the CO transition is overwhelmed by the more "ferromagnetic" response measured in this sample at 240 K.

The magnetization as a function of magnetic field (M-H) for the $La_{0.40}Ca_{0.60}Mn_{0.98}Cr_{0.02}O_3$ sample exhibits a spontaneous magnetization (a sharp "S-shaped" magnetization curve) below 240 K on top of a paramagnetic background response (magnetization increasing linear with the field) similar to the 200 K curve shown in Fig. 2. The magnitude of the spontaneous magnetization (value extrapolated back to zero field) increases with decreasing temperature, while the slope of the paramagnetic background remains fairly constant. Below 150 K, however, the spontaneous magnetization increases more rapidly and a small hysteresis begins to develop between the increasing and decreasing field data at the largest field values. This hysteresis continues to open up with decreasing temperature as seen in the 100 and 50 K data of Fig. 2 with the hysteresis for $H \leq 0.5$ T being much smaller and not readily observable within the resolution of this figure. In fact, the hysteresis at higher field strengths appears to result from the magnetization exhibiting a field-induced increase for increasing fields above 0.5 T as the magnetization increases faster than just in a linear fashion. This hysteresis and field-induced behavior gradually diminish for temperatures below 50 K, and eventually the M-H curve at 5 K becomes more characteristic of a bulklike ferromagnetic material exhibiting a saturation magnetization. However, the measured saturated moment of $1.8\mu_B$/f.u. is about 50% of the expected value of $3.4\mu_B$/f.u. which could indicate that ferrimagnetic phases rather ferromagnetic phases may be present. Thus, the temperature and field dependences of the magnetization for the $y=0.02$ sample suggest that a ferromagnetic ordered phase or region occurs at 240 K which coexists with a paramagnetic phase. This paramagnetic phase then orders below 150 K into another ferromagnetic phase which is characterized by an upturn (increase) in the temperature-dependent magnetization below 150 K, irreversibility between the field-cooled and zero-field-cooled magnetization data, and a field-induced magnetization with increasing magnetic fields. While these magnetic behaviors below 150 K are characteristics of a ferromagnetic cluster glass phase, the lack of any field dependence in the temperature (around 100 K) where the magnetization becomes temperature independent is not typical of a glass freezing temperature.

Fortunately the electrical resistivity as a function of the temperature and magnetic field for the

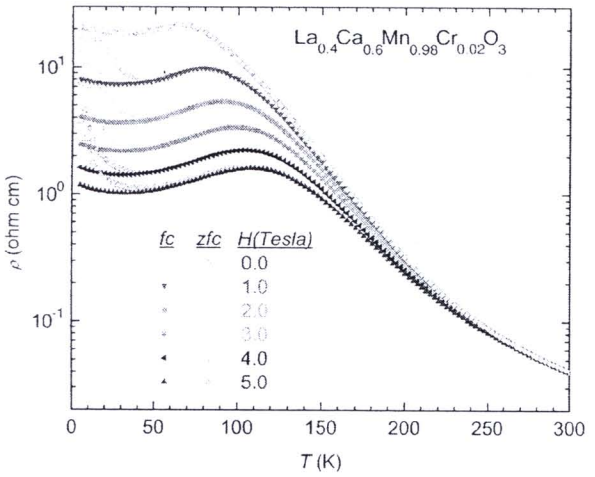

FIG. 3. (Color online) The dc electrical resistivity ρ of $La_{0.40}Ca_{0.60}Mn_{0.98}Cr_{0.02}O_3$ as a function of temperature T. Both the fc and zfc data are shown for different magnetic field strengths H.

$La_{0.40}Ca_{0.60}Mn_{0.98}Cr_{0.02}O_3$ sample provides some additional clues as to the nature of these ferromagnetic phases and transitions, as shown in Fig. 3. The zero-field resistivity initially follows a semiconductorlike temperature dependence starting at room temperature with no visible change in slope around 240 K, then begins to deviate from this semiconductorlike temperature-dependent behavior below 150 K, and eventually forms a plateaulike structure below 70 K. In comparison the resistivity of the undoped material is semiconductinglike over the entire temperature region and shows essentially no magnetic field dependence.[7] However, this characteristic temperature behavior with a plateau for the $y=0.02$ sample is very reminiscent of the resistivity measured for a $Pr_{0.40}Ca_{0.60}Mn_{0.93}Cr_{0.07}O_3$ sample at 7 T,[6] which was interpreted as resulting from a insulator-to-metallic (I/M) transition induced by the applied magnetic field. Moreover, since the present resistivity measurement is in zero applied field, the magnetic field needed to induce such a transition more likely arises from the internal field associated with the ferromagnetic order that occurs at 150 K. Upon the application of a finite magnetic field, a small negative magnetoresistance begins to appear around 240 K which increases in magnitude with decreasing temperature until a much larger negative magnetoresistance is observed below 150 K that is strongly field dependent. With increasing magnetic field strengths, the plateaulike structure forms at higher temperatures as expected since the combined internal and applied fields should induce the I/M (more accurately semimetal) transition to occur at even higher temperatures. Also the field-induced magnetization observed in the M-H curves below 150 K provides additional experimental evidence for the field-induced PMI/FMM transition at 150 K and the resulting large negative magnetoresistance ratio ($R_0/R_{5\,T} \approx 20$) at 5 K. It must be noted, however, that neither the crossover to the plateaulike structure in the zero-field resistivity nor the field-induced behavior in the magnetoresistance is as sharp as the behavior observed in many other Cr-doped manganites exhibiting an I/M transition.[5] Finally at temperatures below 40 K, the magnetoresistance shows a hysteretic behavior between the zero-field-cooled and field-cooled measurements which may also be related to the 40 K bump observed in the temperature-dependent magnetization data at low fields.

With increasing Cr concentration ($y \leq 0.06$), the relative magnitude of the spontaneous magnetizations associated with the 240 and 150 K ferromagnetic phases and the corresponding characteristic temperature of their appearance decrease. Likewise the M-H curves for the $y=0.04$ and 0.06 samples (not shown) are very similar to those of the $y=0.02$ sample including field-induced characteristics at temperatures below 150 K.

Also the zero-field electrical resistance for these Cr-doped samples follows a similar semiconductorlike temperature dependent behavior with the deviation to the plateaulike structure occurring at progressively lower temperatures with increasing Cr concentration.

In summary, polycrystalline samples of $La_{0.40}Ca_{0.60}Mn_{1-y}Cr_yO_3$ ($y=0.02-0.06$) have been synthesized and their magnetic and electrical properties investigated. Even with just 2% Cr, the charge ordering transition in the undoped parent composition is completely suppressed as a ferromagnetic ordering accompanied by a negative magnetoresistance occurs at 240 K. At 150 K, a second ferromagnetic phase appears with the electrical and magnetic characteristics of an insulator-to-semimetal transition that can be further induced (enhanced) by an applied magnetic field. Similar phases appear in the other Cr-doped samples ($y \leq 0.06$) although at different temperatures and relative amounts depending on the Cr concentration. The addition of Cr also results in the appearance of a magnetoresistance below the insulator-to-semimetal transition temperature with magnetoresistance ratios ranging from 10^1 to 10^3 at 5 K.

[1]R.-W. Li, J.-R. Sun, Z.-H. Wang, and B.-G. Shen, J. Appl. Phys. **88**, 5924 (2000).
[2]C. Martin, A. Maignan, F. Damay, M. Hervieu, B. Raveau, Z. Jirak, G. André, and F. Bourée, J. Magn. Magn. Mater. **202**, 11 (1999).
[3]A. Barnabé, A. Maignan, M. Hervieu, F. Damay, C. Martin, and B. Raveau, Appl. Phys. Lett. **71**, 3907 (1997).
[4]R. Mahendiran, B. Raveau, M. Hervieu, C. Michel, and A. Maignan, Phys. Rev. B **64**, 064424 (2001).
[5]B. Raveau, A. Maignan, and C. Martin, J. Solid State Chem. **130**, 162 (1997).
[6]A. Barnabé, A. Maignan, M. Hervieu, and B. Raveau, Eur. Phys. J. B **1**, 145 (1998).
[7]X. G. Li, R. K. Zheng, G. Li, H. D. Zhou, R. X. Huang, J. Q. Xie, and Z. D. Wang, Europhys. Lett. **69**, 670 (2002).

การปรับเปลี่ยนพลังงานแถบช่องว่างของทินออกไซด์โดยการแทนที่ด้วย Fe^{3+}

TUNING THE BAND GAP ENERGY OF SNO_2 BY SUBSTITUTION WITH FE^{3+}

ทวีศักดิ์ สุดยอดสุข[1] มาลี ประจวบสุข[1] และ พงศ์ทิพย์ วิโนทัย[2]

Taweesak Sudyoadsuk[1], Malee Prajuabsuk[1] and Pongtip Winotai[2]

[1]Advanced Organic Materials & Devices Laboratory, Department of Chemistry, Faculty of Science, Ubon Ratchathani University, Ubon Ratchathani 34190, Thailand

[2]Department of Chemistry, Mahidol University, Bangkok 10400, Thailand

บทคัดย่อ: ได้เตรียมอนุภาคนาโน $Sn_{1-x}Fe_xO_{2-\delta}$ (x = 0, 0.01, 0.1, 0.2, และ 0.3) โดยเทคนิคออโตคอมบัสชัน และศึกษาการเปลี่ยนแปลงพลังงานแถบชองว่างโดยเทคนิคออปติคัลสเปกโทรสโกปี พบว่าพลังงานแถบช่องว่างของอนุภาคนาโน $Sn_{1-x}Fe_xO_{2-\delta}$ มีค่าลดลงเมื่อปริมาณของตัวเติม Fe เพิ่มขึ้น แสดงให้เห็นว่าเกิดอันตรกิริยาการแลกเปลี่ยนกันระหว่าง d กับ s และ p อิเล็กตรอน

Abstract: The nanoparticles $Sn_{1-x}Fe_xO_{2-\delta}$ (x = 0, 0.01, 0.1, 0.2, and 0.3) samples have been prepared by the auto-combustion technique. The optical spectroscopy has been used to measure the band gap of the samples. The bandgap show a progressive decrease as concentration of Fe increased. The decrease in band gap is attributed to the sp-d exchange interaction.

Introduction: Tin oxide, SnO_2, is a very interesting oxide semiconductor with a wide band gap of ~ 3.6 eV for bulk. Its high optical transparency, electrical conductivity, and chemical sensitivity make it a very attractive material for solar cell, catalysis, and gas sensor applications. The preparation of these materials in the nanoscale size range is more interesting due to the increased surface-to-volume ratio which might affect the structural and physical properties. Doping with transition metal elements has been proposed to introduce magnetic functionally in semiconductor. Recently, diluted magnetic semiconductors (DMS) have been studied extensively due to their potential application to spintronic and optoelectronic devices [1]. Although there have been very few reports on SnO_2-based DMSs compared to other oxide-based DMSs, many properties have been observed, such as a giant magnetic moment, and large coericitivity [2]. Moreover, the origin of magnetism still remains a question [3]. The theoretical study has explained that the strong exchange interaction between d electron of the magnetic transition metal and the s and p electrons of the matrix is a most distinctive feature of DMS [4]. The sp-d exchange interaction effects on the band gap of the semiconductor. In this study, we have investigated the optical band gap variation in the nanoparticles $Sn_{1-x}Fe_xO_{2-\delta}$ (x = 0, 0.01, 0.1, 0.2, and 0.3) samples, prepared by auto-combustion technique.

Methodology: Stoichiometric amounts of $SnCl_4 \cdot 5H_2O$ and $Fe(NO_3)_3 \cdot 6H_2O$ were mixed in a HNO_3 solution with citric acid and ethylene glycol. The mixed solution was heated until a resin material was formed. The obtained resin was then calcined at 700 °C in order to obtain oxide nanoparticles. Powder X-ray diffraction (XRD) measurements were carried out with a X-pert Panalytical diffractometer using CuK_α (1.5418 Å) radiation. Further analysis by the Rietveld method using the FULLPROF program was carried out [5]. The average crystallite sizes were calculated from XRD profile breadth based on Double-Voigt (DV) algorithm using BREADTH program [6]. TEM observation was performed with JEOL JEM 2010

transmission electron microscope. The diffuse reflectance UV-Vis spectrum was recorded by Shimadzu UV-3101PC spectrophotometer

Results, Discussion and Conclusion: The XRD pattern of the $Sn_{1-x}Fe_xO_{2-\delta}$ (x = 0.01, 0.1, and 0.2) and Rietveld refinement diffractograms of $Sn_{0.7}Fe_{0.3}O_{2-\delta}$ are shown in Figure 1. These patterns are indexed to the tetragonal rutile-type structure with the space group *P42/mnm*. No trace of iron metal, oxides or any binary tin-iron phases were observed in any of the doped samples. The XRD intensities showed significant changes as Fe doping. Since the Sn atom has the atomic scattering factor larger than that Fe atom. The decreasing in XRD intensities implies that the Sn sites were substituted by Fe. All the samples have very broad XRD peaks due to their nanocrystalline behavior. The diameters of the nanoparticles were estimated from the breadth of (110) and (211) diffraction peaks. The analysis gives the average crystallite size of 11.2±0.1, 9.6±0.6, 8.1±0.5, 7.7±0.5 and 6.3±0.3 nm for x = 0, 0.01, 0.1, 0.2 and 0.3, respectively. The particle size decreased with Fe doping, in excellent agreement with TEM studies, as show in Figure 2(a). However, the particles size estimated from TEM is slightly larger than that obtained from XRD breadth. TEM image of $Sn_{0.7}Fe_{0.3}O_{2-\delta}$ sample showed nearly rectangular-like nanoparticles (Figure 2(b)).

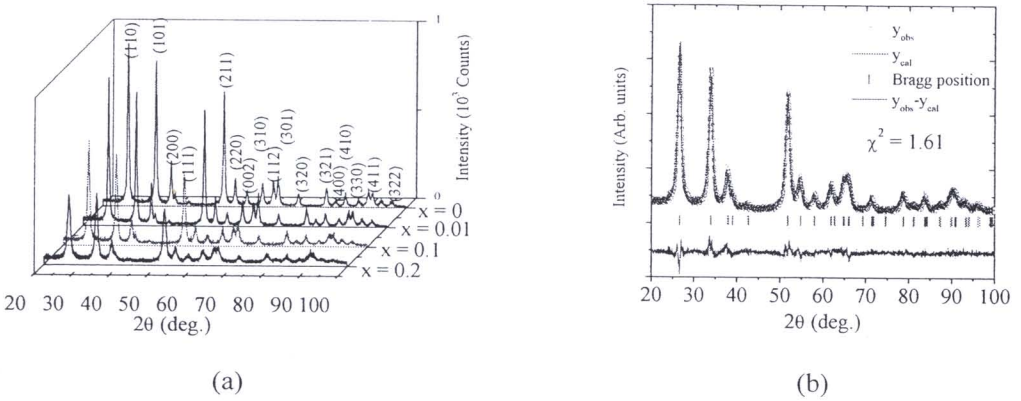

Figure 1. (a) XRD patterns of $Sn_{1-x}Fe_xO_{2-\delta}$ (x = 0.01, 0.1, and 0.2) (b) Rietveld refinement XRD diffractogram of $Sn_{0.7}Fe_{0.3}O_{2-\delta}$

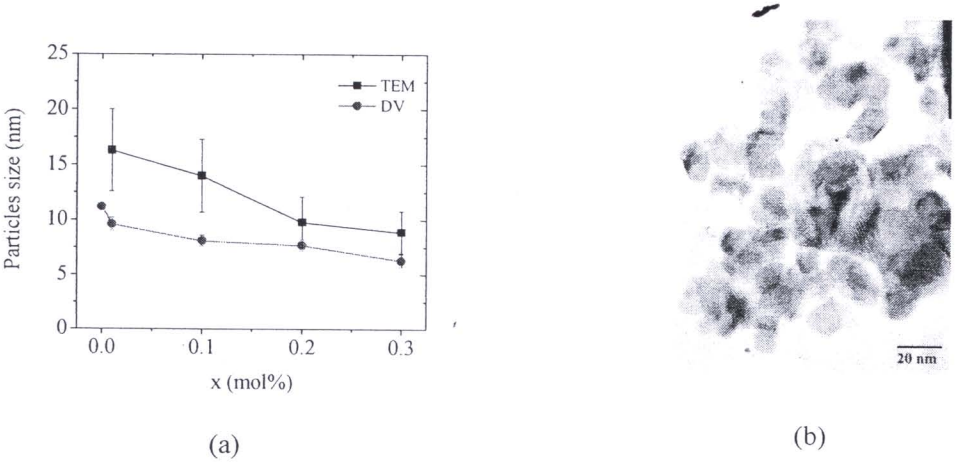

Figure 2. (a) Particles size of $Sn_{1-x}Fe_xO_{2-\delta}$ as function of x calculated from DV algorithm and determined from TEM (b) TEM image of $Sn_{0.9}Fe_{0.1}O_{2-\delta}$

The diffuse reflectance spectra for nanoparticles samples are shown in Figure 3(a). The shoulders at 450 nm is ascribable to d-d transition of Fe(III) ion in octahedral field. The diffuse reflectance, R is related to the Kubelka-Munk function $F(R)$ by the relation $F(R) = (1-R^2)/2R$. The band gap energies were then calculated from plotting of $F(R)^2$ vs. energy. The linear part of the curve was extrapolated to intercept an abscissa axis to get direct band gap energy. The variation of the band gap with x is given in Figure 3(b). It was found that, the band gap energy decrease with increasing Fe concentration. The decrease in band gap is attributed to the sp-d exchange interaction [4].

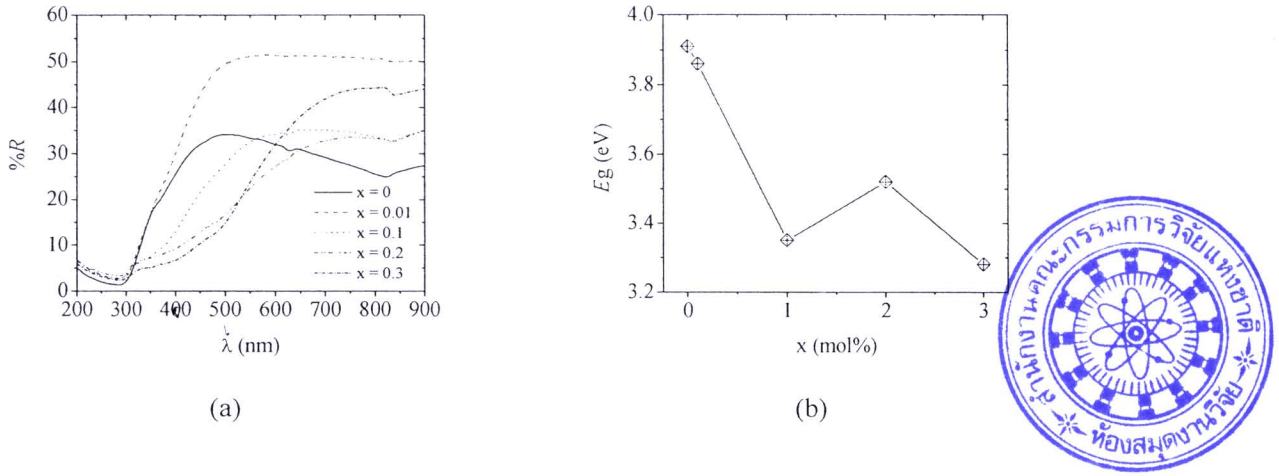

Figure 3. (a) Diffuse reflectance spectra of the $Sn_{1-x}Fe_xO_{2-\delta}$ (b) Shift of band gap energy (Eg) with concentration x.

The present studies show that the band gap energy of nanoparticles Fe^{3+} doped SnO_2, prepared by auto-combustion method, is progressive decrease with the dopant concentration. The bandgap is decreasing by about 0.6 eV for 3% Fe doping.

References:

1. T. Dietl, H. Ohno, F. Matsukura, J. Cibert, and D. Ferrand, *Science*, 2000, **287**, 1019.
2. T. Fukumura, Y. Yamada, H. Toyosaki, T. Hasegawa, H. Hoinuma, and M. Kawasaki, *Appl. Surf. Sci.* 2004, **223**,62.
3. J. M. D. Coey, A. P. Douvalis, C. B. Fitzgerald, and M. Vaenkatesan, *Appl. Phys. Lett.*, 2004, **84**, 1332.
4 S. Venkataprasad Bhat and F. L. Deepak, *Solid State Comm.*, 2005, **135**, 345.
5. J. Rodriguez-Carvajal, *Physica B*, 1993, **192,** 55.
6. D. Balzar and H. Ledbetter, *Advances in X-ray Analysis*, 1997, **39**, 457.

Keywords: nanoparticles, tin oxide, SnO_2, band gap

Acknowledgements: TS acknowledge the Thai Royal Fund (TRF) for Grant No. MRG480056. We would like to thank the Department of Chemistry, Faculty of Science, Khon Kean University for providing UV-Vis spectrophotometer, and the Science and Technology Service Center, Chiang Mai University for providing TEM facilities.